Available on CMS information server

CMS NOTE-2008/003

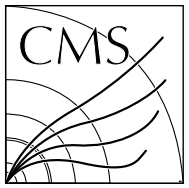

The Compact Muon Solenoid Experiment

CMS Note

Mailing address: CMS CERN, CH-1211 GENEVA 23, Switzerland

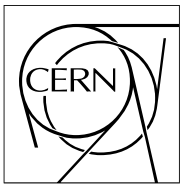

29 January 2007

Measurement of Drift Velocity in the CMS Barrel Muon Chambers at the CMS Magnet Test Cosmic Challenge

M.C.Fouz,C.Villanueva (CIEMAT), R.Carlin,U.Gasparini,A.T.Meneguzzo,M.Zanetti (Padova),
G.Cerminara,S.Bolognesi (Torino)

Abstract

This note reports the results of the analysis performed on the data collected by the CMS Barrel Muon system during the Magnet Test-Cosmic Challenge, aimed to study the Drift Tube chambers behavior at the nominal value of the CMS magnetic field. In particular, the analysis is devoted to the study of the drift velocity in the various equipped regions of the apparatus. It is shown that the drift velocity is significantly affected by the presence of a residual magnetic field in the chamber volume only in the innermost stations, MB1, of Wheel+2; where the maximal variation inside the chamber is of 4 percent, which does not prevent a good functionality of the DT trigger even in this most critical region.

1 Introduction

The CMS Muon Barrel system, described in detail in [1], consists of 4 concentric "station" of 250 chambers inside the magnet return yokes of CMS, which is in turn divided into 5 wheels. A wheel is divided into 12 sectors, each covering a 30^o azimuthal angle. Wheels are labeled consecutively from YB-2 for the furthest wheel in $-z$ to YB+2 for the furthest in $+z$, while sectors are labeled in order of increasing ϕ, beginning with the sector at $\phi = 0$, in which the chambers are in the vertical plane.

In the Summer-Autumn 2006, during the test of the CMS magnet, which for the first time was closed and brought to its design value of B=4 T, a large amount of cosmic rays data was collected. The purpose was to test as much as possible the integration of all the sub-detector components from the point of view of hardware, trigger, DAQ and off-line analysis software, and to study their behaviour in the real experimental environment.

As far as the Barrel Muon system is concerned, a total of 14 DT chambers (i.e., about 5% of the whole Muon Barrel detector) were fully equipped and included in the global CMS DAQ readout system. These stations covered Sector 10 of Wheel+1 and Wheel+2, and Sector 11 of Wheel+2 (i.e. the two sectors in the lowest part of a Wheel, in which the chambers are placed either horizontally or with an inclination of 30^o, thus maximizing the cosmic rays trigger rate), as shown by the contour sketched in Fig. 1. In the same sectors, the Resistive Plate Chambers (RPC) equipping the muon stations [1] were also operational, providing a trigger to CMS independent from the DT system. The 14 DT chambers were operated with an $Ar - CO_2$ (85/15%) gas mixture; the O_2 contamination was kept below 100 ppm. The gas pressure at the chambers' input and output was continously monitored and measured to be stable within ± 2 mbar over the whole data taking period.

In the End-cap part of the apparatus, in correspondence with the Barrel active sectors, 36 Cathode Strip Chambers (CSC) [1] were active, providing another independent muon trigger and participating in the DAQ during the Cosmic Challenge.

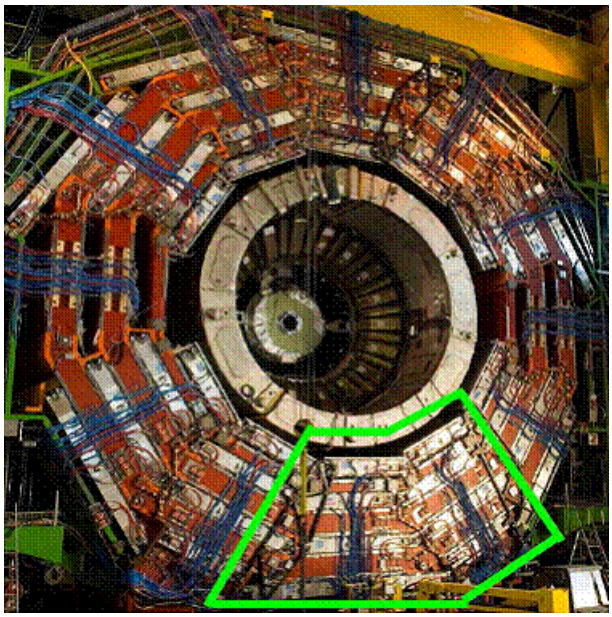

Figure 1: Picture of Wheel+2 (outlined in white), showing the Magnet Test-Cosmic Challenge setup for the Muon Barrel system.

Each DT chamber in the 3 innermost stations, MB1-MB3, consists of 12 layers of drift tubes divided into 3 groups of 4 consecutive layers, hereafter called SuperLayers (SL), as schematically shown in the left part of Fig. 2. Two SLs (hereafter referred to as ϕ-SLs) measure the $r - \phi$ coordinate in the bending plane, and the third SL (referred to as θ-SL) measures the z-coordinate running parallel to the beam. A honeycomb aluminium structure separates a ϕ SL from the other two SLs, thus giving a lever arm of about 30 cm for the measurement of the track direction in the bending plane inside each chamber. The tubes inside each SL are staggered by half a tube. The MB4 chambers have only the 2 SLs for the $r - \phi$ measurement, separated by the honeycomb structure.

The basic detector component inside each chamber, the DT cell, is shown in the right part of Fig. 2. One of its crucial properties is a linear behaviour in the space-time relationship between the detected time of the electronic

signal recorded on the anode wire and the position of the muon passage through the cell. For the purpose of the DT trigger functionality and for the muon track reconstruction, it is essential to control at better than the percent level the drift velocity of the electrons producing the signal on the anode wire. It is known that, in the presence of a residual magnetic field in the cell volume, the lines of force defining the drift path of the electrons are distorted due to the Lorentz force, resulting in a variation of the "effective" drift velocity in the linear space-time relationship.

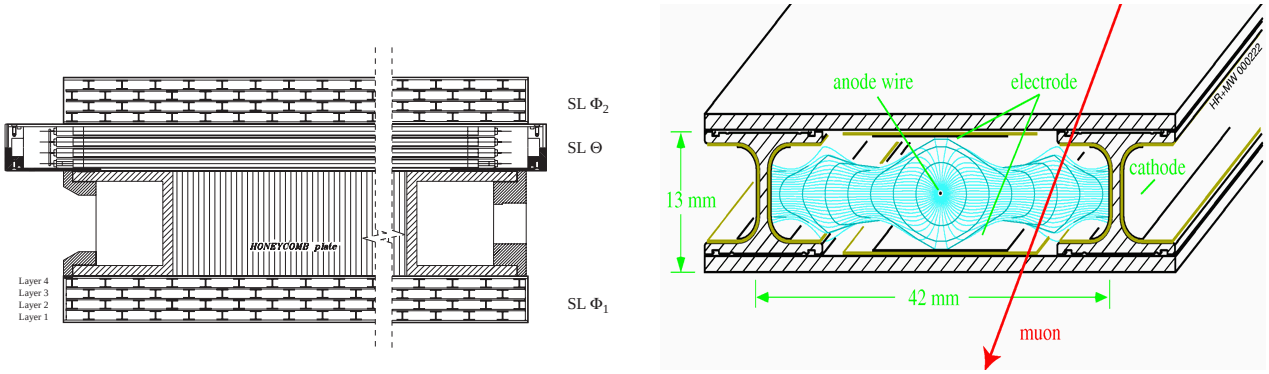

Figure 2: Left: cross-sectional view of a Muon Barrel chamber; right: a drift cell.

As can be seen in Fig. 3, the residual field in the cradles inside the iron yokes where the muon stations are placed can reach considerably high values, particularly in Wheels+2 and -2. Its radial component (i.e., the component perpendicular to the DT wires which is the one most affecting the effective drift velocity) is expected to be as high as 0.8 T in the MB1 regions closest to the CMS endcaps.

Previous tests performed using a small DT prototype [2] in a test beam and under various magnetic field configurations showed that the drift velocity variation was small enough to prevent a significant degradation of the chamber functionality in the presence of such a field. It's thus important to study the behaviour of the full-size chambers in the real CMS environment and confirm this expectation.

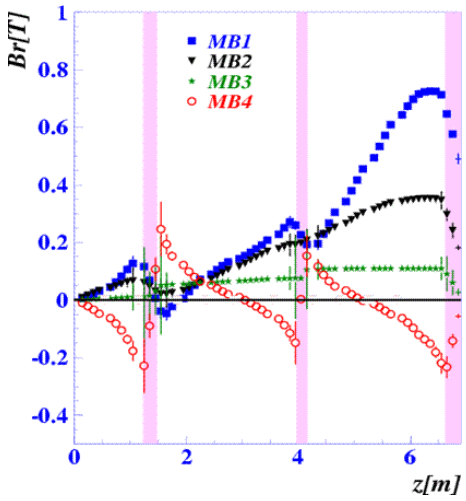

Figure 3: The radial component of the magnetic field in the Muon Barrel chambers for the different wheels, as a function of z.

2 Drift velocity determination from different methods

Three independent methods have been developed for measuring the electron drift velocity in the DT cell. The first is based on the computation of the mean time variable [2], which provides a measurement of the maximum drift time, T_{max}, and hence of the drift velocity, if a linear space-time relation is assumed. The L_{max}/T_{max} ratio, with $L_{max} = 2.1$ cm being the half-cell size, measure the "effective drift velocity" which is used in the first stage of the hit reconstruction, averaged over the DT cell volume and over the different inclinations of the muon tracks. The method relies on a careful determination of the "time pedestal" t_0, i.e., the starting point of the drift

time distribution, defined as the time of passage of a muon passing through the anode wire. Given the strong anti-correlation between the two variables, the uncertainty on the t_0 determination produces a non-negligible systematic error on the value of the drift velocity. However, the method gives good sensitivity for studying the relative variation of the drift velocity under different magnetic field conditions.

The second method is based on the photo-extraction of electrons from the cell's cathode, which typically occurrs under normal DT cell operating conditions in a few percent of the events. As discussed below, this method provides an independent measurement of T_{max} that does not rely on the determination of the time pedestal.

The third method relies on a muon track fit, which determines track-by-track the time of passage of the muon through the chamber and the drift velocity as additional free parameters in the fit, together with the track position and inclination angle.

2.1 The T_{max} method

The "mean-time" is obtained from three consecutive layers, which are staggered half a cell apart, using:

$T_{MT} = (t_j + t_{j+2})/2 + t_{j+1} = T_{max}$

where t_j is the time of arrival, pedestal subtracted, of the electron signal in the j-th layer in a chamber Super-Layer. This variable measures the maximum drift time T_{max} when the muon track passes through the cells of a same column inside the SL structure, i.e., for tracks inclined by less than 40^o with respect to the normal to the chamber plane (the maximum inclination depends on the impact position inside the cell). For operation with bunched beams as at the LHC, this quantity has a Gaussian distribution with a width given by $\sqrt{3/2}$ times the intrinsic time resolution of the DT device, i.e., 5-6 ns (neglecting the time spread of the collisions, the spread of the time of flight of the muon from the collision point to the muon detector, and the signal propagation time along the anode wire; these last two effects can be corrected for using the space information from the two "views" of the DT chamber). In a cosmic rays environment, the T_{max} distribution is significantly broadened by the crossing time of the muon inside the 25 ns window of the time-of arrival identification provided by the trigger, which by design has a bunch-crossing spacing granularity. For a flat- event population distribution, this would give an r.m.s. contribution of $2 \times 25/\sqrt{12} \sim 15$ ns; this value is further modified by the fact that, due to the lack of fine synchronization of the internal clock in the trigger device with the muon crossing (which will be done at the LHC), the efficiency of the trigger response is not uniform within the 25 ns window. Finally, without a relative synchronization of the trigger signals from the different devices (DT, RPC and CSC) operating during the magnet test, the T_{max} distributions may have different average values for different trigger sources, if the same time pedestal subtraction is used. This can be seen in Fig. 4, where typical "raw" mean time distributions for events triggered by different devices are shown for one SL of a MB2 chamber, computed assuming the same time pedestal.

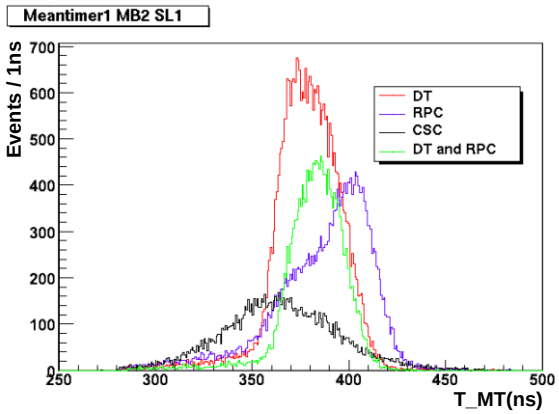

Figure 4: "Raw" Mean Time distributions for the channels in SuyperLayer 1 of one MB2 chamber for different triggering devices.

The time pedestal for the different trigger sources is determined for each SL of chambers by fitting the rising edge of the drift time distribution, as described in detail in [3]. Examples of these distributions are shown in Fig. 5 (left) for the signals in all the cells of a given SL, together with a typical fit from the pedestal calibration procedure (right) [3].

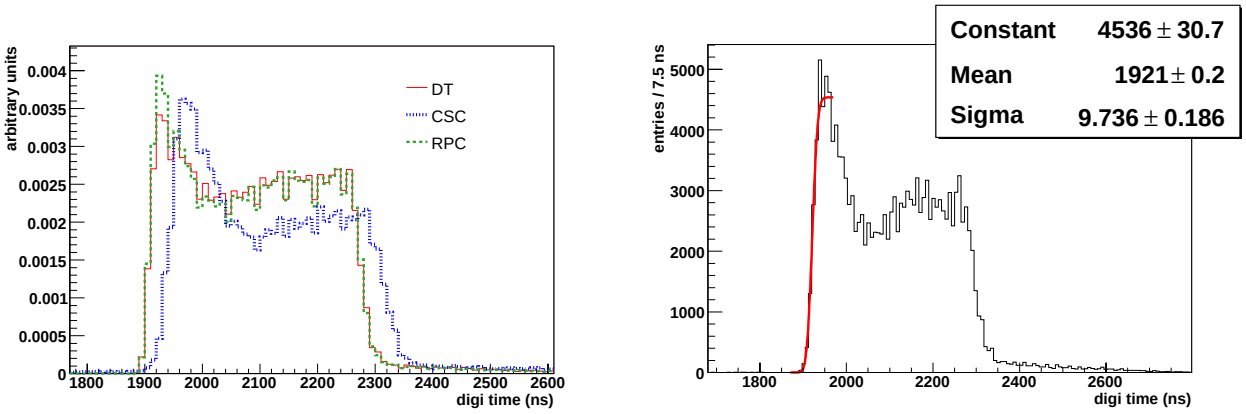

Figure 5: Left: examples of drift time distributions for events triggered by different muon trigger devices; right: time pedestal fit from the calibration procedure.

After the time pedestal calibration is performed independently for each SuperLayer of chambers used in the magnet test and for the different trigger sources, the T_{max} distributions obtained using the data from the ϕ SL's are fitted with a Gaussian in the range $[T_{max,av} - 1.3 \cdot \sigma, T_{max,av} + 1.3 \cdot \sigma]$, where $T_{max,av}$ and σ are the average and the r.m.s. values of the distribution respectively. The data are divided into five different regions (approximately 50 cm wide) along the CMS z-axis, using the information from the θ SL in each chamber, and the average of the Gaussian fit is found. The data at B=0 and B= 4 T are compared. The relative variation of the drift velocity at B= 4 T with respect to the average value measured in each region at B= 0 is shown in Fig. 6 for all chambers. It can be seen that in the MB1 chambers of both sectors of Wheel+2, in which the radial component of the residual magnetic field is expected to be large, there is a sizable variation in the drift velocity, and that the results are independent of the trigger source. This variation amounts to $\sim 3.5\%$ in the region closest to the endcap. In all other chambers the variations, if present, are much smaller and anyway comparable with the sensitivity of the method, although some effects can be seen in the MB2 chambers of Wheel+2, as will be evident from the track fit method discussed in a following section.

The results for the MB1 station in Wheel+2 are in good agreement with those obtained from a test-beam measurement on a chamber prototype, reported in [2]. This can be seen from the comparison shown in Fig. 7, performed using the magnetic field values from the map computation displayed in Fig. 3.

In order to have a more precise definition of the peak of the T_{max} distribution and to further cross-check possible systematic effects on its determination due to the shape of the distribution, the T_{max} computation is modified including a track-by-track correction to the "overall" time pedestal determined by the calibration procedure outlined above. This correction accounts for the time of arrival of the muon inside the trigger time window, using the T_{max} computed for a "reference" SL (the first ϕ SL of MB3, shown in the left part of Fig. 8). One half of the difference between the actual value of T_{max} and the average value of this distribution is used as a correction to the TDC signal times recorded in the other SL's and in the other chambers. The effect of this correction to the T_{max} distribution of the second ϕ-SL of MB3, as seen in the right part of Fig. 8, shows a considerable reduction in the spread of the distribution. This spread is now due to the convolution of the intrinsic DT time resolution and the time of the signal propagation along the wire (which is only partially accounted for by the measurement of the reference SL in MB3, depending on the track inclination). Similar distributions are obtained for the SL's in the other chambers.

The variation of the average T_{max} value due to the signal propagation time along the wire in different regions of a chamber, observed in the data at B=0, is clearly visible in Fig. 9. This variation must be corrected for when measuring the drift velocity needed by the track reconstruction algorithm. The T_{max} values in the regions closest to the front-end electronics side of the chambers (the right-most points for each chamber in the plot), which measure the actual drift velocity, correspond to a drift velocity of $(54.34 \pm 0.05)\mu$m/ns and $(54.55 \pm 0.05)\mu$m/ns for the two MB1 chambers in Wheel+2, and to $(57.28 \pm 0.05)\mu$m/ns for the MB1 chamber in Wheel+1. The quoted errors correspond to the statistical error of the Gaussian fit to the corrected T_{max} distributions. The large difference ($\sim 5\%$) between the values of the drift velocity in Wheel+2 and Wheel+1 is due to the different gas purity in the chambers. Indeed, while the MB1 chambers in Wheel+2 were operated in normal conditions, the MB1 chamber of Wheel+1 was not flushed during the data taking due to a gas distribution problem, causing an increase of nitrogen in the gas mixture.

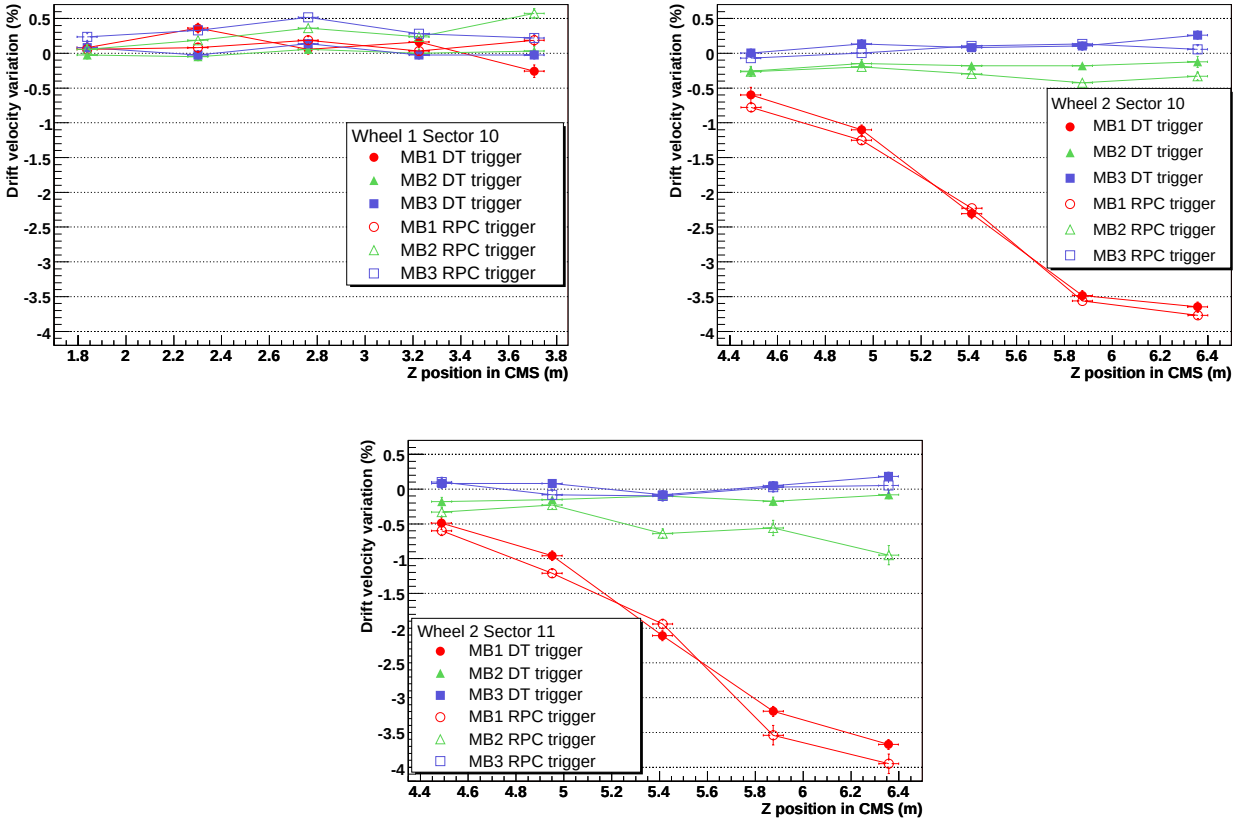

Figure 6: Relative variations of drift velocity (in percent) between B=4 T and B=0 versus z. Upper, left: chambers in Wheel+1; right: Wheel+2, sector 10. Bottom: Wheel+2, sector 11.

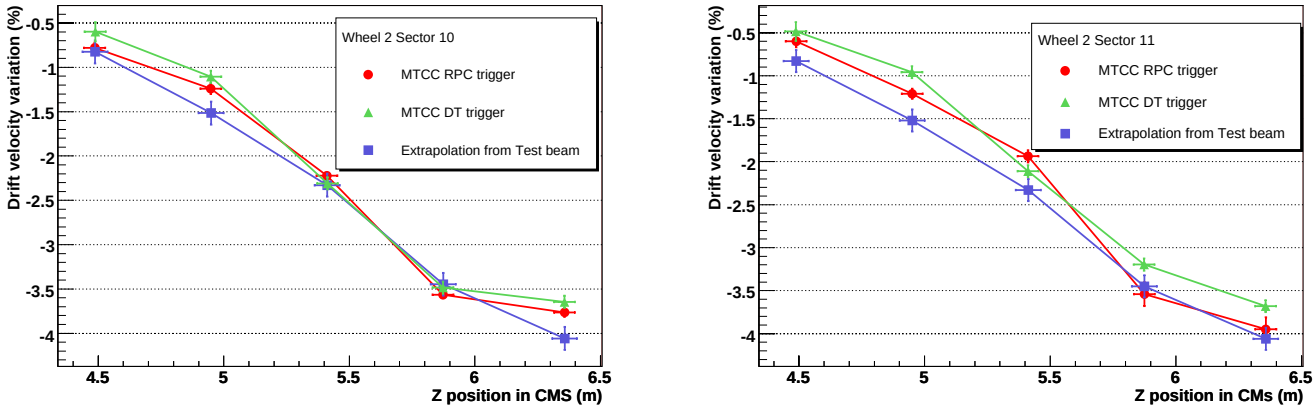

Figure 7: Drift velocity variation (in percent) versus z in MB1 of Wheel+2, computed for different triggers and compared with an extrapolation from test-beam results. Left: Sector 10; right: Sector 11.

The value of the drift velocity at B=4 T in the MB1 chambers, after the appropriate correction is performed for the signal propagation time, is shown in the left part of Fig. 10. It can be seen that the drift velocity is constant (and compatible with the value observed at B=0) in the MB1 chambers of Wheel+1, while it decreases significantly in the MB1 chambers of Wheel+2. The ratio between the values obtained for B = 4 and B=0 T is displayed in the right part of Fig. 10, which shows good agreement with the result given in Fig. 6.

Table 1 summarizes the results on the relative variation between B=4 T and B=0 data as measured in the outermost ϕ-SL of all the chambers in the magnet test, averaged over the SL volumes. The values are also compared with

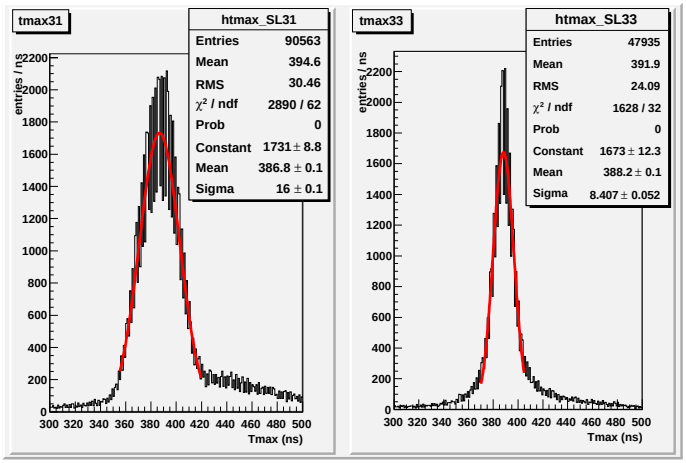

Figure 8: Left: the "raw" Mean Time distribution for MB3, SL1; right: the corrected mean time distribution for MB3, SL3.

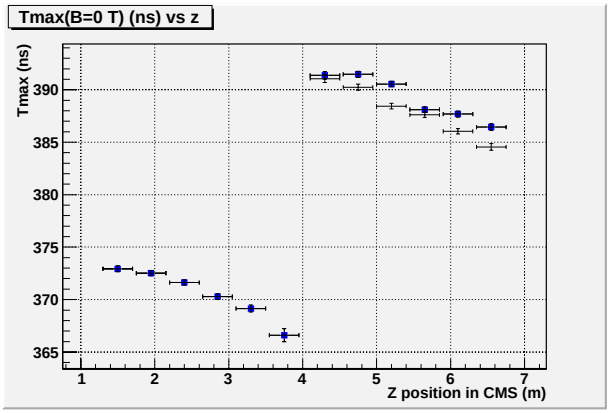

Figure 9: The variation of T_{max} as a function of the muon impact position along the anode wire due to the signal propagation time in B=0 data, observed in the three MB1 chambers. Each chamber is subdivided into six regions. The right-most points in each chamber correspond to the region closest to the front-end electronics side. Squares refer to MB1 chambers in Sector 10; crosses refer to the MB1 chamber in Wheel+2, Sect.11.

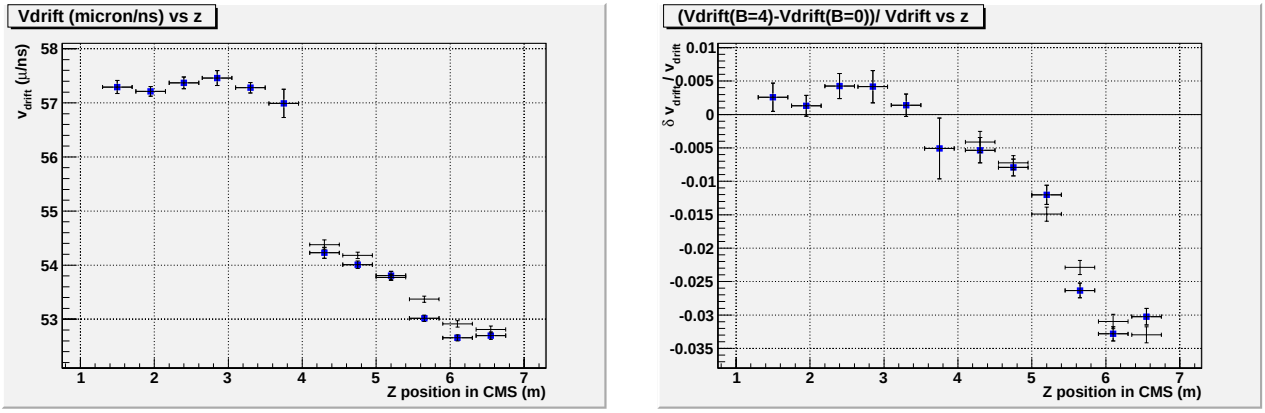

Figure 10: Left: V_{drift} versus z in the three MB1 chambers for B=4 T. Right: relative V_{drift} variation with respect to B=0. Symbols are as in Fig. 9.

those obtained with the other methods discussed in the next sections. The quoted uncertainties are the statistical errors from the fit described above; the systematic error associated with the uncertainty on the time pedestal determination is $\pm 0.2\%$.

Chamber/Wheel/Sector	$\delta v_d/v_d$ (%) with T_{max} method	$\delta v_d/v_d$ (%) with photo-peak method SLΦ_1/ SLΘ/ SLΦ_2	$\delta v_d/v_d$ (%) with track fit method
MB1/W1/S10	0.24 ± 0.07	$0.0 \pm 0.2/0.0 \pm 0.2/0.0 \pm 0.2$	0.50 ± 0.05
MB2/W1/S10	0.05 ± 0.02	$0.4 \pm 0.2/0.0 \pm 0.2/0.0 \pm 0.2$	0.42 ± 0.03
MB3/W1/S10	-0.28 ± 0.04	$0.4 \pm 0.2/0.0 \pm 0.2/-0.4 \pm 0.2$	0.31 ± 0.03
MB4/W1/S10	-0.30 ± 0.09	$0.0 \pm 0.2/-/0.4 \pm 0.2$	0.58 ± 0.05
MB1/W2/S10	-2.05 ± 0.06	$-2.4 \pm 0.2/-2.4 \pm 0.2/-2.4 \pm 0.2$	-1.88 ± 0.05
MB2/W2/S10	-0.38 ± 0.03	$-0.6 \pm 0.2/-1.0 \pm 0.2/-0.8 \pm 0.2$	-0.09 ± 0.03
MB3/W2/S10	-0.03 ± 0.03	$-0.6 \pm 0.2/-0.4 \pm 0.2/-0.6 \pm 0.2$	0.41 ± 0.03
MB4/W2/S10	0.11 ± 0.06	$-0.2 \pm 0.2/-/0.0 \pm 0.2$	0.70 ± 0.05
MB1/W2/S11	-2.67 ± 0.11	$-2.5 \pm 0.2/-2.8 \pm 0.2/-2.4 \pm 0.2$	-1.72 ± 0.05
MB2/W2/S11	-0.30 ± 0.03	$-0.4 \pm 0.2/-0.6 \pm 0.2/-0.8 \pm 0.2$	0.22 ± 0.03
MB3/W2/S11	-0.05 ± 0.03	$-0.2 \pm 0.2/0.0 \pm 0.2/0.0 \pm 0.2$	0.27 ± 0.03
MB4/W2/S11	0.25 ± 0.05	$-0.4 \pm 0.2/-/-0.2 \pm 0.2$	-0.07 ± 0.05

Table 1: Relative variation of the drift velocity between B=0 and B=4 T data (in percent), averaged over the chamber volume, for chambers used in the magnet test. The values from the T_{max} method refer to the outermost ϕ SL's (SLΦ_2) in the chambers. Quoted errors are statistical only. The systematic error associated with the uncertainty on the time pedestal determination is $\pm 0.2\%$. For the photo-peak method, the average values obtained for each of the three superlayers in a chamber are quoted separately (MB4 chambers have only two ϕ SL's). The values from the track fit method refer, by definition, to the entire chamber.

2.2 The photo-peak method

The primary electrons which are strongly accelerated in the avalanche region near the anode wire produce photons that can extract secondary electrons from the cathode strips and I-beams of the cell. The latter drift along the entire cell volume, causing a signal at a time T_{max} after the occurence of the primary electron signal due to the passage of the muon. An example of this signal is shown by the narrow peak in Fig. 11, which displays the distribution of the time difference between the primary and the secondary electron signals (the time binning of the TDC was set to 0.781 ns/count). The broad peak around 250 TDC counts originates from the electrons extracted from the strips below the anode wires, which drift along a shorter path in the DT cell; an additional small contribution is expected from electron δ-rays delivering hits starting after the dead time of the TDC+Front End amplifier.

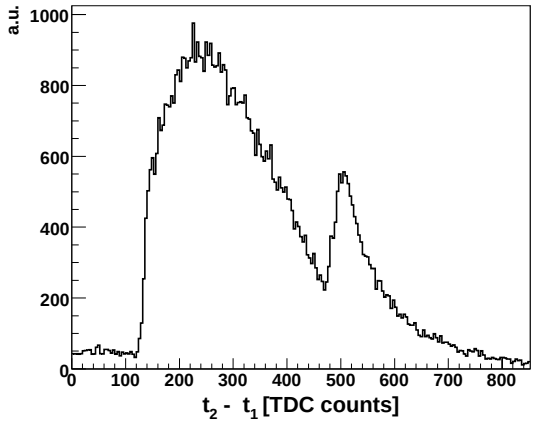

Figure 11: Distribution of the time difference between the primary and secondary electron signals, for all the cells in a superlayer. The photo-peak signal caused by the electrons extracted from the cell I-beams is clearly visible at $\sim$510 TDC counts.

Figure 12 shows the distributions of the photo-peak signal, enlarged in the time region of interest, for one MB1 chamber of Wheel+2 for data at B=0 and B=4 T. The shift of the photo-peak position towards larger values of the time difference for B=4 T is clearly visible, showing a decrease of the drift velocity, averaged over the chamber volume, of about 2.5%.

In Fig. 13 the variation of the photo-peak position along the z axis in the local reference frame of the chamber is

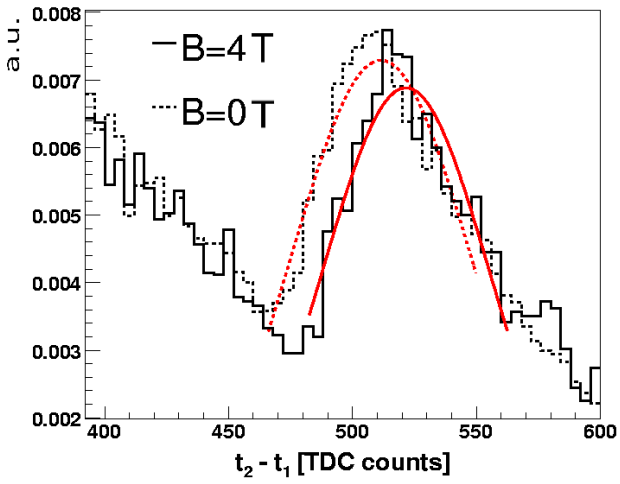

Figure 12: Photo-peak signals in an MB1 chamber of Wheel+2 for two B field values.

shown; the behaviour is in good agreement with the variation of the drift velocity observed with the T_{max} method.

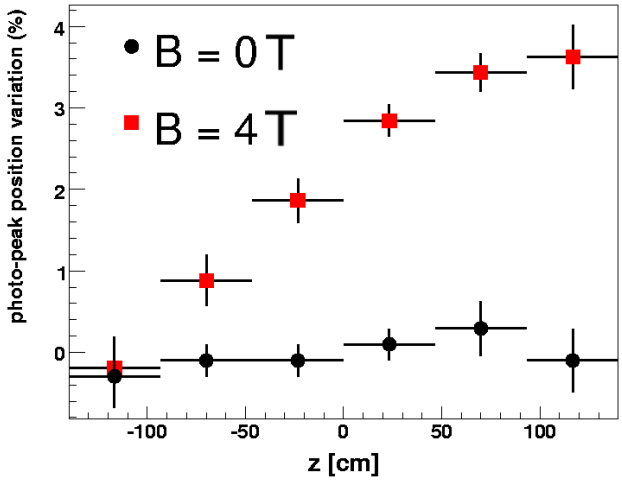

Figure 13: Relative variation, in percent, of the photo-peak position as a function of z in the chamber for two magnetic field values, as measured in the MB1/Wheel+2 chamber.

Table 1 summarizes the results of the relative variation between the B=4 T and B=0 data for the different SL's of all chambers used in the magnet test. The values are averaged over the SL volumes. As observed with the T_{max} method, only the MB1 chambers in Wheel+2 show a significant difference between the two sets of data.

2.3 The track fit method

As explained in Section 2.1, the time of arrival distribution of cosmic ray tracks has an intrinsic spread of $(25/\sqrt{12})$ ns (the mean-time quantity defined in that section has a spread twice larger). Since a muon produces up to 8 points (in a large majority of events) in the ϕ view of each DT chamber, it is possible to perform a straight-line fit to the reconstructed hits, leaving the time of passage of the muon and the drift velocity as additional free parameters in the fit, together with the track impact position and direction [4]. This is done after a preliminary reconstruction step is performed, which reconstructs the hits using a "nominal" value for the drift velocity (set to 54.3 μm/ns, i.e., the average value observed using the T_{max} method at B=0 for the MB1 chambers in Wheel+2). The reconstruction performs a pattern recognition algorithm which finds the hits belonging to a muon track candidate [5]. The method, different from the one based on the T_{max} computation, does not require a careful chamber-by-chamber calibration

of the time pedestal; in fact, for all the chambers in a given sector the same time pedestal calibration is used.

After the fitting procedure, the residuals of the reconstructed hits with respect to the extrapolated position from the track fit are considerably reduced, as shown in Fig. 14. The resolution obtained, on the order of ~ 200 μm, is comparable with the one expected from the intrinsic time resolution of the DT cell, as measured from test-beam data.

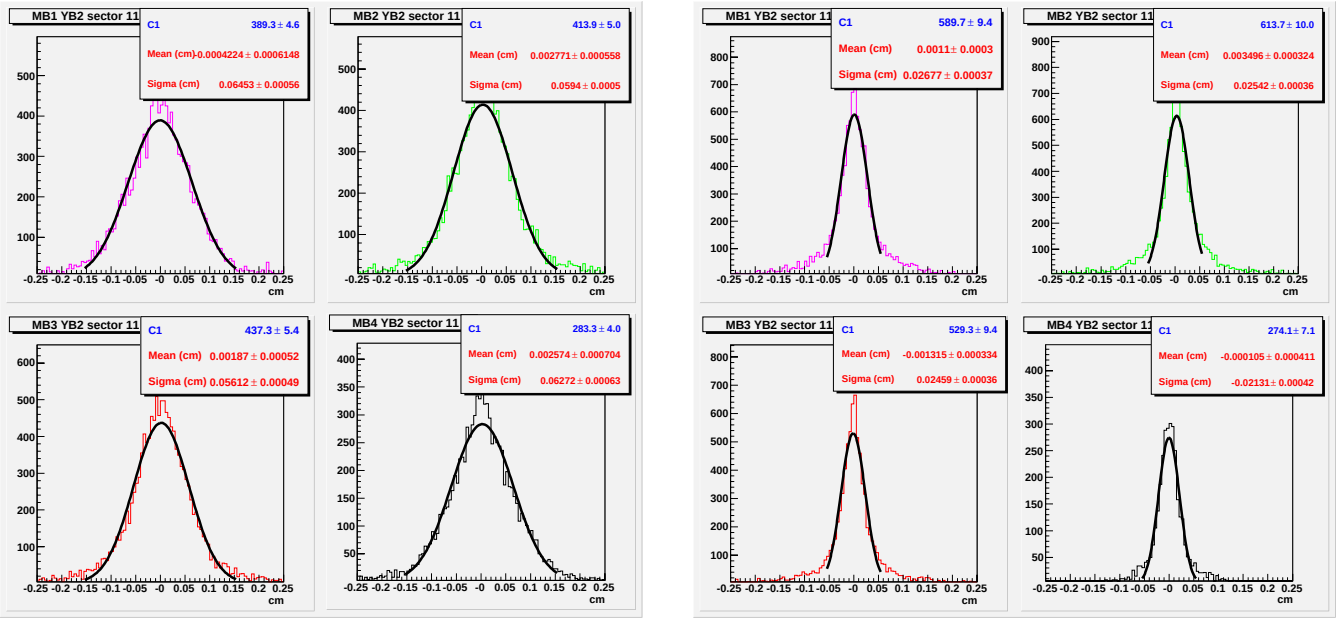

Figure 14: Reconstructed hit residuals (cm) with respect to the extrapolated position from the track fit, for the four chambers in Sector 10 of Wheel+2. Left: using a 2-parameter straight line fit; right: using a 4-parameter fit which includes the determination of the muon time of passage and of the drift velocity.

Figure 15 shows in the right plot the distribution of the relative corrections to the nominal value of the drift velocity, obtained for the B=0 data of the MB1 chamber in Wheel+1. The shift of $\sim 6\%$ in the average value of the distribution is compatible with the difference observed with the T_{max} method. The distribution obtained for the muon time of passage is shown in the left plot of the figure. Its spread, ~ 10 ns, is quite compatible with the expectation from the time of arrival of the muon inside the 25 ns trigger window.

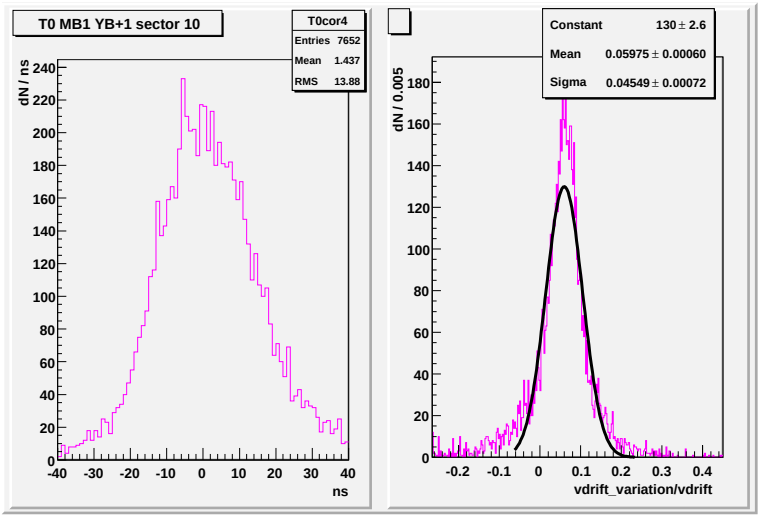

Figure 15: Left: distribution of the fitted values of the muon time of passage, for muon tracks crossing the MB1 station in Wheel+1. Right: distribution of the relative correction to the nominal value of the drift velocity obtained from the track fit.

The result of the drift velocity fits as a function of the muon track position along the CMS z axis is shown in Fig. 16 for the chambers of Sector 10 in Wheel+1 using the B=4 T data. The plots show the average value of the distribution for a given position interval; the error bars give the r.m.s. of the distribution (not the error on the average). The drift velocity is constant throughout the entire chamber volume, in agreement with the previous observations. The average value of the correction for MB1, 6.3%, gives a value for the drift velocity of $(57.72 \pm 0.05)\mu$m /ns (significantly different from the values from the other chambers due to the already mentioned gas distribution problem in this chamber). The difference ($\sim 0.7\%$) with the value obtained for this chamber with the one from the T_{max} method ($(57.3 \pm 0.05)\mu$m /ns, see left plot in Fig. 10), is compatible with the systematic error expected from the time pedestal definition in the latter.

Figure 17 shows the results of the drift velocity fits for the chambers in Sectors 10 and 11 of Wheel+2; in this case a decrease of the drift velocity in the MB1 chambers and, to a smaller extent, in MB2 is clearly evident as the track position gets into regions of higher residual magnetic field values. The overall variation in the MB1 chambers is on the order of $\sim 3\%$, ranging from 54.8 μm/ns to 52.9 μm/ns, again very compatible with the measurements from the T_{max} method, shown in Fig. 10.

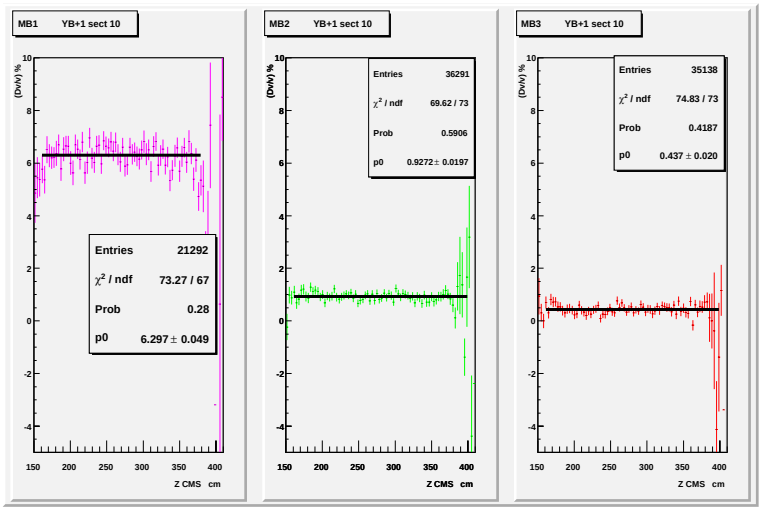

Figure 16: Variation along z of the drift velocity w.r.t. the nominal value as measured from the track fitting method, for chambers in Wheel+1, at B=4 T. Left: MB1, center: MB2, right: MB3.

Finally, the behaviour of the chambers was studied in runs with different values of the magnetic field, during various scans used for the magnetic field mapping. The results of the relative variation in the drift velocity per unit length along the z axis (the slope of the fits in Fig. 17) are shown in Fig. 18 for the MB1 chambers in Wheel+2. It can be seen that values of $(\Delta v/v)/dz$ greater than (1%)/m are reached for magnetic fields larger than 3.5 T. The error bars are the systematic errors (the statistical error from the fitting procedure being negligible), conservately evaluated condidering the maximum variation obtained for chambers MB2 and MB3, in which the effect of the residual magnetic field is negligible.

It is interesting to test the stability of the measurement of the average drift velocity in the MB1 station of Wheel+1 (where the effect of the magnetic field is negligible). This is shown in Fig. 19. The different measurements span several days of chamber operations with no input gas. Although specific studies of chamber operation without gas flow were not performed, the stability of the drift velocity is an indication of the good hermeticity of the chamber, with little variation in gas purity.

3 Summary and conclusions

The behaviour of the DT chambers in the Muon Barrel system during the CMS Magnet Test and Cosmic Challenge was extensively studied, in particular for what concerns the determination of the electron drift velocity in the different regions of the apparatus, for data taken at the nominal value of the CMS magnetic field.

Using cosmic rays data recorded in the Cosmic Challenge, the results obtained for DT chambers in the environment of the CMS experiment confirm the measurements performed using test-beam data on a small chamber prototype. The observed variations of the drift velocity, even in the most critical regions of the apparatus (the innermost

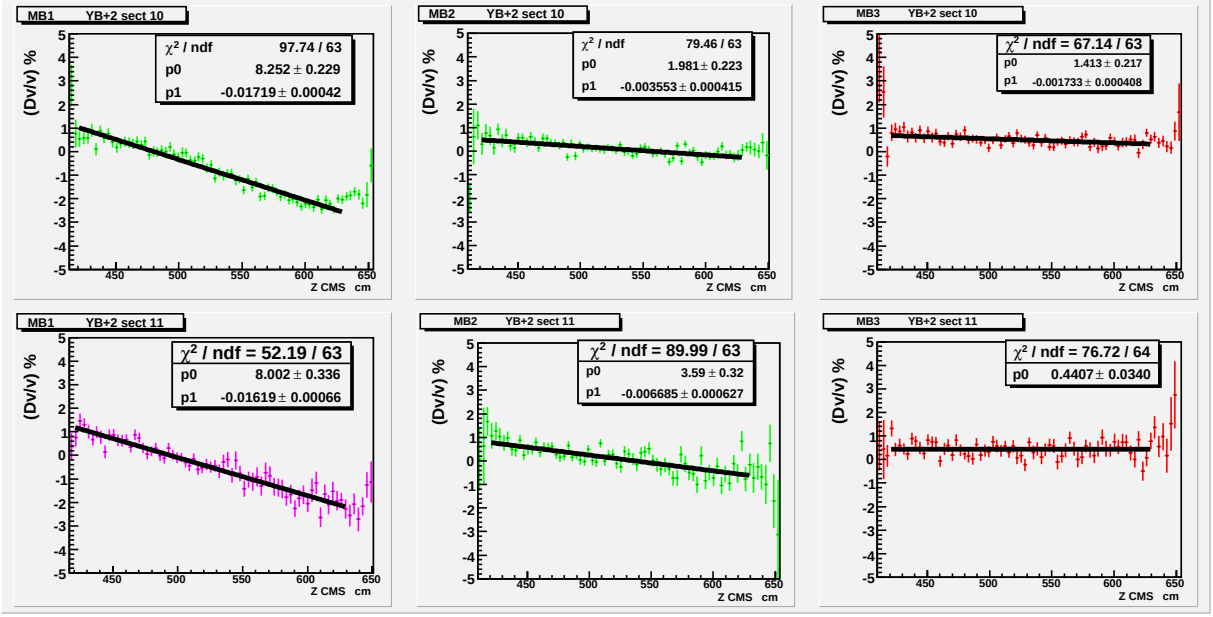

Figure 17: Relative variations (in percent) of the drift velocity along the z axis with respect to the nominal value (54.3 μm/ns) as measured from the track fitting method in chambers of Wheel+2. Upper plots: Sector 10; lower plots: Sector 11.

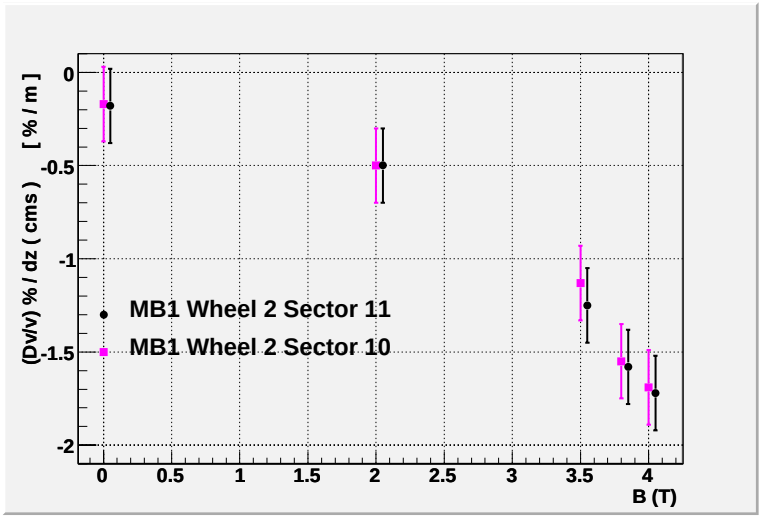

Figure 18: Relative drift velocity variation per unit length along the z-axis, in percent, for 2 MB1 chambers in Wheel+2, as a function of the magnetic field.

chambers in the Wheels closest to the endcaps), are within the tolerance required for the trigger functionality of the DT system.

The procedures and algorithms described in this note can be used in fast online monitoring of the drift velocity and trigger latency, and in High Level Trigger processing for good track reconstruction, even in the case of an inaccurate calibration of the time pedestal and drift velocity.

References

[1] The Muon project Technical Design Report, CERN/LHCC 97-32.

[2] M.Aguilar-Benitez et al.,“Study of magnetic field effects in drift tubes for the barrel muon chambers of the CMS detector at the LHC”, Nucl. Instr. and Meth. A 416 (1998), 243-252.

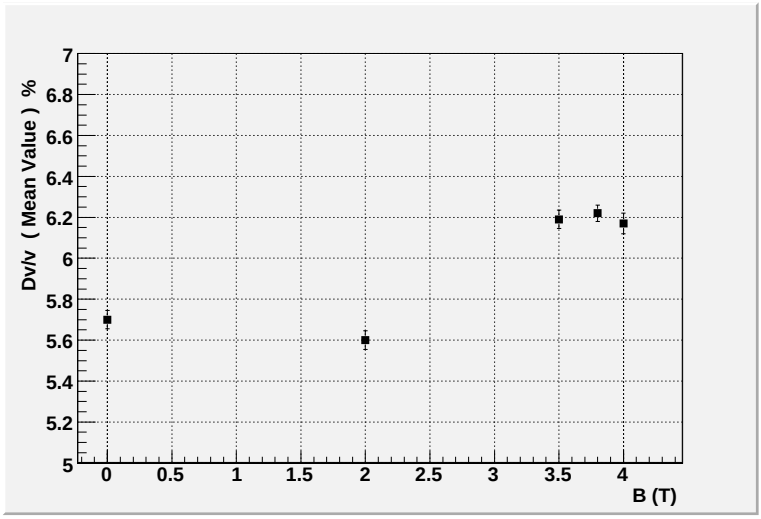

Figure 19: Relative drift velocity variation, in percent, in the MB1 chamber of Wheel+1 for different values of the magnetic field. The data were taken over a period of several days, showing the stability of the drift velocity.

[3] N.Amapane et al.,“Offline Calibration Procedure of the Drift Tube Detector”, CMS NOTE 2007/034.

[4] The Muon track segment fit in CMSSW, https://uimon.cern.ch/twiki/bin/view/CMS/T0Seg.

[5] The Object Reconstruction for CMS Analysis program (CMSSW), http://cmsdoc.cern.ch/CMSSW/; the Muon software in CMSSW, https://uimon.cern.ch/twiki/bin/view/CMS/MuonSW.